Modelling the Stepped Potential Discharge of Primary Alkaline Battery Cathodes

J.F. Johansen & T.W. Farrell

Mathematical Sciences, Queensland University of Technology, GPO Box 2432, Brisbane QLD 4001, Australia

Abstract

A novel model for the potentiostatic discharge of primary alkaline battery cathodes is presented. The model is used to simulate discharges resulting from the stepped potential electrochemical spectroscopy (SPECS) of primary alkaline battery cathodes cathodes, and the results are validated with experimental data. We show that a model based on a single (or mean) reaction framework can be used to simulate multi-reaction discharge behaviour and we develop a consistent functional modification to the kinetic equation of the model that allows for this to occur. The model is used to investigate the effects that the initial exchange current density, i_0^0, and the diffusion coefficient for protons in electrolytic manganese dioxide (EMD), D_{H^+}, have on SPECS discharge. The behaviour observed is consistent with the idea that individual reduction reactions, within the multi-reaction, reduction behaviour of EMD, have distinct i_0^0 and D_{H^+} values.

Introduction

In essence, the cathode of a primary alkaline battery is formed by compressing small, porous particles of electrolytic manganese dioxide (EMD) and graphite together into a steel can and flooding the resulting porous solid with aqueous potassium hydroxide (KOH) electrolyte. The effect of this is to produce a porous electrode, which, during discharge undergoes non-linear and interconnected physical, chemical and electrochemical processes.

This discharge is characterized by the reduction of EMD; a complex process that proceeds via the intercalation of H^+ ions into its crystal structure, converting MnO_2 into $Mn(OH)_2$. Several attempts have been made to characterise this process[1–8]. The most comprehensive of these accounts is due to Chabre and Pannetier[8] who found that EMD reduction consists of a mixture of heterogeneous and homogeneous processes, some of which are irreversible. In particular, these authors found that the crystal structure of EMD is irreversibly distorted during reduction and that the onset of such distortion occurs at different times, depending on how close the EMD is to equilibrium during discharge.

Chabre[7] and Chabre and Pannetier[8] used Step Potential Electrochemical Spectroscopy (SPECS) to examine the reduction process in EMD. In a SPECS discharge, the cell is subjected to a series of consecutive potentiostatic discharges, in which the cell potential is decreased (or stepped) by a fixed amount in each discharge (usually starting near the OCV), and the current response is recorded. The advantage of SPECS over other continuous discharge modes such as galvanostatic, constant load, or constant power is that it emphasizes the electrochemical and physical responses of the cell. Ideally, the cell is given time to equilibrate at each potential level, thus minimising transport losses. However, this means that individual SPECS discharges can take many days to complete.

The multi-reaction nature of the reduction of EMD is very apparent in the SPECS results. The minimum and maximum current or power experienced during each potentiostatic discharge, versus potential, are frequently used to visualise the results of a SPECS discharge. Such data (as we shall

see below) displays several clearly visible peaks which are attributable to the reactions that constitute the reduction process[7,8], and clearly show that it is not a single reaction process.

Understanding the behaviour of complex systems, like batteries, is essential to their cost effective improvement as they do not always behave intuitively. Mathematical modelling can be used to extend our understanding of these complex systems, although in primary alkaline batteries, for example, the difficulty in characterising the reduction process of EMD presents a challenge to such modelling. To accurately model such a process, the full reaction mechanism, including rate constants at well characterised reference conditions for each individual reaction should be known. Without the appropriate information approximations must be made and the modelling of such a process must start at a simpler level. Thus, in contrast to the conclusions drawn by some of the researchers who have experimentally studied the reduction of EMD, the prevailing approach in the mathematical modelling literature[9–19] is to assume that reduction is essentially characterised by a single (mean) reaction, originally proposed by Kozawa and Powers[20], namely,

$$\mathrm{MnO_2 + H_2O + e^- \rightleftharpoons MnOOH + OH^-}\,. \tag{1}$$

Assuming this, a single current-overpotential characteristic (usually a Butler-Volmer type expression) may be used to describe the kinetics at the EMD/KOH interface, and a single Nernst expression may be adopted to describe the zero current potential or open circuit voltage (OCV).

In adopting this simplified approach to modelling EMD reduction it has been widely realised[8,21–23] that the Nernst equation that ensues from Reaction (1) must be modified in order to produce OCV curves that are closer to those observed experimentally. For example, Chabre and Pannetier[8] propose the modified Nernst equation,

$$E = E^{\theta} - \Upsilon\left(C_{\mathrm{Mn^{4+}}}\right) - \frac{R_{\mathrm{gas}}T}{F}\ln\frac{C_{\mathrm{Mn^{3+}}}}{C_{\mathrm{Mn^{4+}}}}, \tag{2}$$

as an approximation of the equilibrium potential for the first electron reduction of EMD. Here E (V) is the equilibrium potential of Reaction (1), E^{θ} (V) is the standard potential for the reaction, $\Upsilon\left(C_{\mathrm{Mn}^{4+}}\right)$ (V) is an unknown concentration dependent term, named the "ion-ion interaction term", that accounts for the difference in the equilibrium potential given by the Nernst equation and that observed experimentally, R_{gas} (J/K.mol) is the universal gas constant, T (K) is the temperature, F (C/mol) is Faraday's constant, and C_i (mol/cm^3) is the concentration of species i.

The incorporation of such modified zero current potential expressions in mathematical models of the closed circuit voltage should be done in a consistent manner; in that, the current-overpotential expressions used in these models should reflect the modified zero current expression adopted when equilibrium conditions prevail at the reaction interface. Such consistency has not always been the case in the previous modelling literature (see e.g. Refs. [9,10,14,15]) for EMD discharge. Importantly, however, even when such consistency is displayed in the modelling of EMD reduction (see e.g. Refs. [16–19]), the true multi-reaction nature of the reduction process remains unaccounted for, which means that such models are inadequate for accurately predicting the SPECS response of alkaline battery cathodes.

A question thus arises as to whether a modelling framework centred on the single, mean reaction reduction mechanism (1) can display multi-reaction behaviour? In this paper we show that this can indeed be achieved and that furthermore, it is the form given to the ion-ion interaction term, $\Upsilon\left(C_{\mathrm{Mn}^{4+}}\right)$, that allows this to occur. We investigate the constraints on this function and the impact that it's form has on the simulation of SPECS discharge using a multi-scale mathematical model. We validate the model output against SPECS experimental data and consider the effect that two key model parameters have on the simulation of SPECS tests.

Model Development & Solution Approach

The model developed here is adapted from the simplified, multi-scale model for the discharge

of primary alkaline battery cathodes previously developed by the authors[18,19]. These equations are based on a cathodic structure, originally proposed by Farrell, Please, McElwain and Swinkels[16], which involves representing the porous cathode using three distinct size scales, as shown in Fig. 1. The sub-microscopic (or crystal) scale consists of nonporous, spherical manganese oxide crystals of a uniform size. Reaction (1) is assumed to occur at the surface of these crystals. These manganese oxide crystals are assumed to be tightly packed and to form porous spherical particles of a uniform size and it is these structures that constitute the microscopic (or particle) scale. The macroscopic (or cathodic) scale is a porous structure, assumed here to be of planar geometry, that consists of porous particles (as described by the microscopic scale) surrounded by a continuous graphite phase that (electronically) connects the particles to the current collector. The porous networks on the cathodic and particle scales are assumed to be saturated with concentrated KOH electrolyte solution and furthermore, the cathode is assumed to be in contact with a reservoir of excess KOH at the $x = 0$ boundary.

Johansen, Farrell and Please[18], based on the previous work of Farrell et al.[16] and Farrell and Please[17], developed a simplified mathematical model for the galvanostatic discharge of the porous cathode structure described above. These authors applied Laplace transform and perturbation methods to the multi-scale model of Farrell et al.[16] to obtain a closed form expression for the concentration of Mn^{4+} ions on the crystal scale (see Eq. (3) below) and to show that for a wide range of industrially relevant discharge conditions the time taken for KOH electrolyte to diffuse into a porous electrolytic manganese dioxide particle is fast compared with the cathodic discharge time and that ohmic losses within the graphite phase of the cathode can be considered to be negligible. The adaptation of this model framework to account for potentiostatic discharge is readily achieved by replacing the galvanostatic discharge condition, imparted by a boundary condition on the current density in the electrolyte phase at the cathode/current collector interface ($x = L$ in Fig. 1), with an appropriate potentiostatic condition (see Eq. (17) below). Noting this, we obtain the following system of crystal, particle and cathode scale equations and associated boundary conditions.

Crystal scale.–

$$C_{\mathrm{Mn^{4+}}} = C^0_{\mathrm{Mn^{4+}}} + \int_{t^*=0}^{t} \frac{3 i_n}{F y_\mathrm{o}}\, dt^* + \sum_{m=1}^{\infty} \frac{2\sin\left(\lambda_m \frac{y}{y_\mathrm{o}}\right)}{F y_\mathrm{o} \sin\left(\lambda_m\right)} \int_{t^*=0}^{t} i_n \left(t - t^*\right) \exp\left\{\frac{-\lambda_m^2 D_{\mathrm{H^+}} t^*}{y_\mathrm{o}^2}\right\} dt^* \tag{3}$$

At $y = y_o$

$$i_n = i_0^0 \left\{ \left(\frac{1 - C^{\mathrm{out}}_{\mathrm{Mn^{4+}}} \bar{V}_{\mathrm{Mn^{3+}}}}{1 - C^0_{\mathrm{Mn^{4+}}} \bar{V}_{\mathrm{Mn^{3+}}}}\right) \left(\frac{C_e}{C_e^0}\right) \exp\left[\frac{\alpha_a F}{R_\mathrm{gas} T}\left(\eta_{(p)} + \Upsilon - \Upsilon^0\right)\right] - \left(\frac{C^{\mathrm{out}}_{\mathrm{Mn^{4+}}}}{C^0_{\mathrm{Mn^{4+}}}}\right) \left(\frac{1 - C_e \bar{V}_e}{1 - C_e^0 \bar{V}_e}\right) \exp\left[\frac{-\alpha_c F}{R_\mathrm{gas} T}\left(\eta_{(p)} + \Upsilon - \Upsilon^0\right)\right] \right\}. \tag{4}$$

Here, $C_{\mathrm{Mn^{4+}}}$ (mol/cm^3) is the concentration of $\mathrm{Mn^{4+}}$ ions per total unit volume on the crystal scale, superscript "0" represents the initial ($t = 0\,\mathrm{s}$) value of the parameter, t (s) is time, t^* is a dummy variable, i_n (A/cm^2) is the transfer current density from oxide phase to electrolyte phase, y (cm) is the radial coordinate on the crystal scale, y_o (cm) is the outer radius of the manganese oxide crystals, $D_{\mathrm{H^+}}$ (cm^2/s) is the diffusion coefficient of $\mathrm{H^+}$ in manganese oxide, which is assumed to be constant, i_0^0 (A/cm^2) is the initial exchange current density of Reaction (1), $C^{\mathrm{out}}_{\mathrm{Mn^{4+}}}$ (mol/cm^3) is the value of $C_{\mathrm{Mn^{4+}}}$ at the outer radius ($y = y_o$) of the oxide crystal, $\bar{V}_{\mathrm{Mn^{3+}}}$ and $\bar{V}_e$ (cm^3/mol) are the partial molar volumes of MnOOH and KOH, respectively, and $\eta_{(p)}$ (V) and C_e (mol/cm^3) are the local overpotential on the porous particle scale and the electrolyte concentration on the cathodic scale, respectively, and are defined by the particle and cathodic scale equations that follow, α_a and α_c are the anodic and cathodic transfer coefficients, respectively and $\Upsilon(C_{\mathrm{Mn^{4+}}})$ (V) is an ion-ion interaction term[8] as discussed previously in relation to Eq. (2). The functional form of this term will be discussed in detail in the following section. Furthermore, the values of λ_m ($m = 1, 2, \ldots, \infty$)

in Eq. (3), are given by the positive roots of[18]

$$\tan(\lambda_m) - \lambda_m = 0. \tag{5}$$

It is important to note that Eq. (4) has been derived in such a way (see[16]) that it defines i_n in terms of a well characterized reference state for the electrode, namely, the equilibrium state that prevails initially ($t = 0\,\mathrm{s}$), prior to any discharge. As such, the exchange current density, , i_0^0, which appears in Eq. (4) and corresponds to the single (mean) reduction reaction (1), is a function of the solid and solution phase concentrations within the cathode at this reference state. Given that all concentrations are assumed to be initially uniform (constant) this then means that i_0^0 is a constant. Furthermore, we note that this infers consistency between Eq. (2) and Eq. (4), in that, Eq. (4) implies Eq. (2) when equilibrium conditions prevail at the reaction interfaces within the cathode.

Particle scale.–

$$\frac{1}{r^2}\frac{\partial}{\partial r}\left(r^2 i_{e(p)}\right) = \frac{3\left(1-\varepsilon_{s(p)}\right)}{y_o} i_n \tag{6}$$

$$\frac{\partial \eta_{(p)}}{\partial r} = i_{e(p)}\left[\frac{1}{\sigma_{\mathrm{EMD}}} + \frac{1}{\kappa_{e(p)}}\right] \tag{7}$$

At $r = 0$

$$\frac{\partial \eta_{(p)}}{\partial r} = 0. \tag{8}$$

At $r = r_o$

$$\eta_{(p)} = \eta. \tag{9}$$

Here, r (cm) is the radial coordinate on the particle scale, r_o (cm) is the outer radius of the porous particle, $i_{e(p)}$ ($\mathrm{A/cm^2}$) is the current per unit cross-sectional area of solution phase on the particle scale, $\varepsilon_{s(p)}$ is the fraction of particle volume that is void due to pores and η (V) is the local over-

potential on the cathodic scale. The effective conductivities of the manganese oxide phase, σ_{EMD} ($\mathrm{S.cm^{-1}}$), and the electrolyte phase on the particle scale, $\kappa_{e(p)}$ (S/cm), are given by

$$\sigma_{\mathrm{EMD}} = k_2 \left(1 - \varepsilon_{s(p)}\right) \left(\frac{C_{\mathrm{Mn^{4+}}}\big|_{y=0.8y_o}}{C^0_{\mathrm{Mn^{4+}}}} \right)^{k_3} \tag{10}$$

and

$$\kappa_{e(p)} = \kappa_{e\infty} \sqrt{\varepsilon^3_{s(p)}}\,, \tag{11}$$

respectively, where k_2 (S/cm) and k_3 are constants and $\kappa_{e\infty}$ (S/cm) is the KOH conductivity in a bulk solution devoid of any porous structure (and is given by expression [A-2] in Ref. [16]).

Cathode scale.–

$$\frac{\partial i_e}{\partial x} = \frac{3\varepsilon_{\mathrm{EMD}}}{\left(1 - \varepsilon_{s(p)}\right) r_o}\, i_{e(p)}\big|_{r=r_o} \tag{12}$$

$$\left(\varepsilon_s + \frac{\varepsilon_{\mathrm{EMD}}\varepsilon_{s(p)}}{1 - \varepsilon_{s(p)}}\right) \frac{\partial C_e}{\partial t} = \frac{\partial}{\partial x}\left[D_{e\infty}\varepsilon_s \frac{\partial C_e}{\partial x} - C_e v^{\square} \right] - \frac{3\varepsilon_{\mathrm{EMD}} t^{\square}_{\mathrm{K^+}}}{\left(1 - \varepsilon_{s(p)}\right) r_o F}\, i_{e(p)}\big|_{r=r_o} \tag{13}$$

$$v^{\square} = \frac{\left(\bar{V}_{\mathrm{H_2O}} - t^{\square}_{\mathrm{K^+}} \bar{V}_e\right)}{F} i_e \tag{14}$$

$$\frac{\partial \eta}{\partial x} = \frac{i_e}{\kappa_e} + \frac{2R_{\mathrm{gas}}T}{F} \left(t^{\square}_{\mathrm{K^+}} + \frac{C_e \bar{V}_{\mathrm{H_2O}}}{1 - C_e \bar{V}_e} \right) \frac{1}{a_e} \frac{\partial a_e}{\partial C_e} \frac{\partial C_e}{\partial x} \tag{15}$$

At $x = 0$

$$C_e = C^0_e \tag{16}$$

and

$$\eta = E_{\mathrm{cell}}(t) - E^0. \tag{17}$$

At $x = L$

$$\frac{\partial C_e}{\partial x} = 0 \tag{18}$$

and

$$i_e = 0. \tag{19}$$

At $t = 0$

$$C_e = C_e^0. \tag{20}$$

Here, i_e (A/cm^2) is the current per unit cross-sectional area of solution phase on the cathodic scale, x (cm) is the spatial coordinate on the cathodic scale, $\varepsilon_{\mathrm{EMD}}$ is the volume fraction of EMD on the cathodic scale, ε_s is the fraction of cathode volume that is void due to spaces between manganese oxide and/or graphite particles, $D_{e\infty}$ (cm^2/s) is the diffusion coefficient of KOH electrolyte in a bulk solution devoid of any porous structure (and is given by expression [A-1] in Ref. [16]), $v^{\square}$ (cm/s) is the volume-average velocity on the cathodic scale, $t^{\square}_{\mathrm{K^+}}$ is the transference number for $\mathrm{K^+}$, $\bar{V}_{\mathrm{H_2O}}$ (cm^3/mol) is the partial molar volume of $\mathrm{H_2O}$, η (V) is the local overpotential on the cathodic scale, κ_e (S/cm) is the effective conductivity of the electrolyte on the cathode scale (and is given by the analogous cathodic form of Eq. (11)), a_e (mol/cm^3) is the activity of the KOH electrolyte solution (and is given by expressions [A-3] to [A-5] in Ref. [16]), $E_{\mathrm{cell}}(t)$ (V) is the applied cell potential (governed here by the SPECS profile) and E^0 (V) is the cell potential at a well defined reference state (here taken to be the equilibrium condition that prevails prior to any discharge of the cathode at $t = 0\,\mathrm{s}$).

Solution approach.– The governing equations and associated boundary conditions are solved numerically by applying a finite-volume method[24] in which they are discretised in space, on either the particle or cathode size scales, and in time. The expression for the electrochemical reaction (given by Eq. (4)) is fully linearized whilst all other nonlinear terms are handled using fixed-point iteration[25]. The time discretrisation can be adjusted via the use of a weighting parameter from fully explicit to fully implicit. The solution is implemented in an extensive program using MATLAB®. The numerical algorithm used to solve the equation system steps through time and iteratively refines the solution of the discretised system of equations at each time step. If this iteration process does not converge then a smaller time step is chosen until it does. The adaptive nature of the time stepping

makes the method robust over a wide parameter range. The simulation time is generally several orders of magnitude smaller than an actual experiment. For example, a SPECS cathodic discharge running from 1.65 V to 0.9 V in steps of 5 mV per hour, takes less than 20 minutes on a standard desktop PC.

Model Parameters & Determining $\Upsilon\left(C_{\mathrm{Mn}^{4+}}\right)$

The cell geometry and discharge parameters that are used in all of the model simulations presented in this work are given in Table 1. These parameters are those of a button cell cathode configuration developed and used by Delta EMD Australia Pty. Limited to test the discharge characteristics of their EMD. Furthermore, the experimental SPECS result used in this work for model validation purposes, and shown in the graphs that follow, was obtained by discharging such a button cell cell and was supplied by Delta EMD Australia Pty. Limited. The remaining model parameters (apart from the ion-ion interaction term, Υ) have been assigned the values, unless otherwise noted, given in Table 2. These values are representative of an industrially relevant manganese oxide and the experimental setup described above.

As an initial test of the model, we simulated a SPECS discharge using a linear form for $\Upsilon\left(C_{\mathrm{Mn}^{4+}}\right)$, namely,

$$\Upsilon = 0.35\left(1 - C^{\mathrm{out}}_{\mathrm{Mn}^{4+}}\bar{V}_{\mathrm{Mn}^{3+}}\right). \tag{21}$$

The comparison of the model output with experimental data is shown in Fig. 2. We observe that the model output compares poorly with the experimental data. The model output does not display any multi-reaction behaviour, as there is only one peak, while the experimental data has at least two clearly evident peaks, one at 1.46 V and the other at 1.3 V. We note that the third peak at 1.12 V may be due to the reduction of pyrolusite, however, it appears to be obscured by additional effects and will not be considered further here.

Improving the approximation of the ion-ion interaction term to yield multi-reaction behaviour is not a straightforward task. However, there are some constraints on the choice of possible approximations. One constraint is that the domain of $\Upsilon\left(C_{\mathrm{Mn}^{4+}}\right)$ must be within realistic Mn^{4+} concentrations. In addition, its range should be positive, because a negative range would increase the zero current potential predicted by Eq. (2) to above those predicted by a standard Nernst equation corresponding to Reaction (1) (i.e. Eq. (2) with $\Upsilon\left(C_{\mathrm{Mn}^{4+}}\right) = 0$), which already overpredicts the experimentally observed zero current potential. Furthermore, we assume that the standard potential, E^0 (V), in Eq. (2) accounts for the initial value of the ion-ion interaction term, $\Upsilon^0 = \Upsilon\left(C^0_{\mathrm{Mn}^{4+}}\right)$, when the initial open circuit voltage is measured. Based on this, the value of Υ^0 is chosen to be zero.

To investigate the effect that the form of $\Upsilon\left(C_{\mathrm{Mn}^{4+}}\right)$ has on the simulation results we now consider using the experimental data provided by Delta EMD Australia Pty. Limited to give an estimate of such a form. To do this we must relate the current predicted by Eq.(4) to the current measured in the SPECS discharge. This requires us to make several simplifying assumptions, which are detailed as follows.

Firstly, we must assume that the concentration distributions within the cathode are close to uniform at the end of each potentiostatic discharge. This assumption may be poor, especially if the time at which the potential is maintained constant is short. Secondly, we assume that each potential step occurs instantaneously, so that the concentration distributions before and after the potential step are the same. Thirdly, we assume that ohmic losses in both the solid and solution phases are negligible. This assumption is also likely to be poor, especially at the later stages of discharge, as reduced EMD has a high ohmic resistance. This assumption, however, is necessary because it allows us to specify that any change in the cell potential is exactly reflected by a change in the particle scale overpotential, $\eta_{(p)}$, at all points in the cathode.

If we admit these assumptions, we may relate the increase in the experimentally observed current

at each potential step to the difference, Δi_n, between the transfer current densities determined by two Butler-Volmer like expressions; one for the transfer current density before, and one after, the potential step. Noting that the concentration terms in the Butler-Volmer expressions remain the same before and after the potential step, because of the first two assumptions, we obtain that,

$$\begin{aligned}\frac{\Delta i_n}{i_0^0} = &\left(\frac{1-\bar{C}^{\text{out}}_{\text{Mn}^{4+}}\bar{V}_{\text{Mn}^{3+}}}{1-C^0_{\text{Mn}^{4+}}\bar{V}_{\text{Mn}^{3+}}}\right)\left(\frac{\bar{C}_e}{C_e^0}\right)\exp\left[\frac{(\alpha_a)\,F}{R_{\text{gas}}T}\left(\bar{\eta}_{(p)}-\Delta E_{\text{cell}}+\Upsilon\right)\right]\\ &-\left(\frac{\bar{C}^{\text{out}}_{\text{Mn}^{4+}}}{C^0_{\text{Mn}^{4+}}}\right)\left(\frac{1-\bar{C}_e\bar{V}_e}{1-C_e^0\bar{V}_e}\right)\exp\left[\frac{-\alpha_{\text{c}}F}{R_{\text{gas}}T}\left(\bar{\eta}_{(p)}-\Delta E_{\text{cell}}+\Upsilon\right)\right]\\ &-\left(\frac{1-\bar{C}^{\text{out}}_{\text{Mn}^{4+}}\bar{V}_{\text{Mn}^{3+}}}{1-C^0_{\text{Mn}^{4+}}\bar{V}_{\text{Mn}^{3+}}}\right)\left(\frac{\bar{C}_e}{C_e^0}\right)\exp\left[\frac{(\alpha_a)\,F}{R_{\text{gas}}T}\left(\bar{\eta}_{(p)}+\Upsilon\right)\right]\\ &+\left(\frac{\bar{C}^{\text{out}}_{\text{Mn}^{4+}}}{C^0_{\text{Mn}^{4+}}}\right)\left(\frac{1-\bar{C}_e\bar{V}_e}{1-C_e^0\bar{V}_e}\right)\exp\left[\frac{-\alpha_{\text{c}}F}{R_{\text{gas}}T}\left(\bar{\eta}_{(p)}+\Upsilon\right)\right]. \quad (22)\end{aligned}$$

Here ΔE_{cell} (V) is the size of the applied potential step, $\bar{\eta}_{(p)}$ (V) is the average particle scale overpotential of the cathode immediately prior to the potential step and $\bar{C}^{\text{out}}_{\text{Mn}^{4+}}$ and $\bar{C}_e$ (mol/cm^3) are the average Mn^{4+} concentration at $y = y_o$ of the cathode and the average electrolyte concentration of the cathode, respectively. These concentrations are also calculated immediately prior to the potential step, however, as noted earlier, they are assumed to be equal to the corresponding concentrations immediately after the potential step. Solving Eq. (22) for Υ at each potential step, we obtain a number of estimates at different Mn^{4+} concentrations.

A polynomial approximation for $\Upsilon\left(C_{\text{Mn}^{4+}}\right)$, based on the above process is shown in Fig. 3. The maximum and minimum power outputs for the corresponding 5 mV/hr SPECS simulation are shown in Fig. 4. The previously introduced experimental 5 mV/hr SPECS results are also shown in Fig. 4. Comparing Figs. 2 and 4 we see that the form of $\Upsilon\left(C_{\text{Mn}^{4+}}\right)$ has a significant effect on the output of the SPECS simulation. Thus, the choice of this function would seem crucial to successfully simulating multi-reaction reduction behaviour in a single reaction modelling framework. Furthermore, from Fig. 4 we observe that the model output based on the $\Upsilon\left(C_{\text{Mn}^{4+}}\right)$ function shown in Fig. 3,

does display two prominent peaks, one at 1.52 V, and another at 1.3 V. Overall, however, the model output does not correspond well with the experimental SPECS discharge.

We note that due to the very interconnected nature of the phenomena that govern cathodic discharge, the parameter values used in the model simulations impact, sometimes significantly, on the prediction of Υ, when determined in the above manner. For example, changing the value of the initial exchange current density, i_0^0, can significantly affect the predicted expression for Υ. As some cell parameters are not measured and there is a level of uncertainty in the values of these parameters, this, along with the above simplifying assumptions that that are made in order to facilitate the fitting process, make it difficult to extract accurate predictions for $\Upsilon\left(C_{\mathrm{Mn}^{4+}}\right)$ from the experimental data in the above manner.

It is important to note, however, that the above analysis was not futile as it facilitates two crucial observations in linking the form of $\Upsilon\left(C_{\mathrm{Mn}^{4+}}\right)$ to the observed multi-reaction discharge behaviour and the successful simulation of SPECS discharge. The first is that the "plateaus" in the $\Upsilon\left(C_{\mathrm{Mn}^{4+}}\right)$ function observed in in Fig. 3 at Mn^{4+} concentrations of 0.042 and 0.012 $\mathrm{mol/cm^3}$, correspond to the peaks in the simulated SPECS discharge in Fig. 4 at 1.52 and 1.3 V, respectively. We note that plateaus at high Mn^{4+} concentrations are reached earlier in the reduction of the oxide and their effects appear in simulated SPECS discharges at higher voltages than plateaus at low Mn^{4+} concentrations. The second observation is that the width of each plateau corresponds to the size of the predicted peak in the simulated SPECS discharge.

Given these observations, we propose the general functional form for $\Upsilon\left(C_{\mathrm{Mn}^{4+}}\right)$ given by,

$$\Upsilon\left(C_{\mathrm{Mn}^{4+}}\right)=\sum_{i=1}^{n}\frac{h_i}{\pi}\left[\arctan\left(s_i\left(C_{\mathrm{Mn}^{4+}}-C_{\mathrm{Mn}^{4+},i}\right)\right)-\arctan\left(s_i\left(C^0_{\mathrm{Mn}^{4+}}-C_{\mathrm{Mn}^{4+},i}\right)\right)\right], \tag{23}$$

as being able to represent the essential features that convey accurate multi-reaction behaviour in

the SPECS discharge simulations whilst not admitting unwanted effects, such as the oscillations associated with higher order polynomials, for example. In Eq. (23), h_i (V) controls the magnitude of the arctan terms, $C_{\mathrm{Mn}^{4+},i}$ (mol/cm^3) denotes the approximate Mn^{4+} concentration at which the corresponding plateau occurs, and s_i controls the slope of the arctan function and how quickly it flattens off to create a plateau. The second arctan function ensures that the value of Υ^0 is zero. Eq. (23) is able to naturally represent each plateau with a single term in the sum, and does not cause unwanted numerical oscillations in our model output. In practice, a satisfactory form for $\Upsilon\left(C_{\mathrm{Mn}^{4+}}\right)$ can be obtained using only three terms in the above sum. Such a form is shown in Fig. 5. A corresponding 5 mV/hr SPECS discharge using this $\Upsilon\left(C_{\mathrm{Mn}^{4+}}\right)$ is compared to the relevant experimental data in Fig. 6. We note that the model output shows a main peak at 1.29 V, with a secondary peak or shoulder at 1.45 V. These correspond well with the position and width of the peaks in the experimental data. However, the magnitudes (heights) of both peaks at 1.29V and the maximum power peak at 1.45V shows only reasonable correspondence with those seen in the experimental data. Through continued refinement of Eq. (23) it may be possible to increase the accuracy of the simulated results, although, we note that the values of i_0^0 and the D_{H^+} are also very important for obtaining the agreement seen in Fig. 6. The fact that in our single reaction modelling framework we are only able to assign a single i_0^0 value may be the primary reason preventing a more accurate model outcome in Fig. 6. To investigate this further we turn our attention to the influences that i_0^0 and the D_{H^+} have on the SPECS discharge behaviour.

Discussion

The initial exchange current density.– i_0^0 (A/cm^2), which appears in Eq. (4), describes the facility of charge transfer at the EMD/KOH interface. It directly affects the size of the current response to changes in the potential and chemical concentrations involved in the reduction of EMD. However, we note that a representative i_0^0 is difficult to obtain experimentally.

The effect of different i_0^0 values on the current response, over three potential steps in a 5 mV/hr SPECS simulation, is displayed in Fig. 7, where the model output is also compared with the relevant experimental data. We observe that the value of i_0^0 significantly affects the current spike at each step in the potential. For small values of i_0^0, for example $5{\times}10^{-9}\,\mathrm{A/cm^2}$, the resulting current spikes are small, while for larger values of i_0^0, for example $5{\times}10^{-7}\,\mathrm{A/cm^2}$, the current response is much more pronounced. In addition to this, the initial exchange current density also affects the rate of relaxation. This is less intuitive than its effect on the initial current spike, however, it may be explained by considering the crystal scale. When i_0^0 is small, protons are inserted at the surface of the EMD crystals at a slow rate, and are able to be transported away from the crystal surface faster than they are inserted. This corresponds to a situation that is kinetically limited, and leads to a more uniform, or flat, current response. For larger values of i_0^0, protons are able to be inserted into the EMD crystals faster than they can diffuse from the surface. This corresponds to a situation where the reduction process is diffusion limited, and leads to larger current responses that diminish quickly. Based on this, we observe that the two 5 mV/hr SPECS simulations with i_0^0 values of $5{\times}10^{-8}$ and $5{\times}10^{-7}\,\mathrm{A/cm^2}$ are both diffusion limited. Interestingly, the experimental data seems to match the model predictions for an i_0^0 value of $5{\times}10^{-7}\,\mathrm{A/cm^2}$ for the first half of each potentiostatic discharge, and seems to match the model predictions for an i_0^0 value of $5{\times}10^{-9}\,\mathrm{A/cm^2}$ for the remainder of each potentiostatic discharge. This would suggest that there are multiple i_0^0 values in the experimental data. This would be consistent with a multiple reaction picture in which, throughout any given discharge step, various reduction processes are occurring preferentially at different times (which is consistent with the work of Chabre and Pannetier[8]), and may be why a better fit was not obtained using a single, constant i_0^0 value.

The effect of i_0^0 on the overall discharge behaviour for simulated 5 mV/hr SPECS discharges is shown in Fig. 8. The fluctuations seen in the data corresponding to the model output for an i_0^0 value of $5{\times}10^{-7}\,\mathrm{A/cm^2}$ are caused by the difficulty the model code has in numerically resolving the extremely thin current spikes observed at large i_0^0 values. This aside, we observe that as the value of

i_0^0 is increased the difference between the observed minimum and maximum power is also increased. This is consistent with our observations of the current response displayed in Fig. 7. However, we do note that this effect is diminished near the end of discharge, below approximately 1.15 V. This is because at the late stages of this discharge the EMD is almost completely reduced and there is simply not enough active material to produce a noticeable current response.

In each of the results shown in Fig. 7 and Fig. 8 we have not varied the form for $\Upsilon\left(C_{\mathrm{Mn}^{4+}}\right)$ from that shown in Fig. 5. In doing this, we have implicitly assumed that there is not a strong functional relationship between the value of i_0^0 and a given value of $\Upsilon\left(C_{\mathrm{Mn}^{4+}}\right)$. It is important to note that such an assumption does not impact upon the outcome from Fig. 7, namely; that, given that i_0^0 is a constant in our model (associated with a single (mean) reaction), we are unable to match the experimental current decay curves for the entirety of each discharge step and that this is consistent with the idea that there are multiple i_0^0 values in the experimental data, each associated with one of the multiple reduction processes.

Revisiting Fig. 6, and considering in particular the comparison of the experimental data with the model output using the form of Υ shown in Fig. 5, we see that there is a larger difference between the minimum and maximum power for the shoulder peak at 1.45 V in the experimental data than there is for the main peak at 1.29 V. In the context of a multi-reaction reduction process, this suggests that the dominant reduction process occurring at 1.45 V has a larger i_0^0 than the dominant reduction process occurring at 1.29 V.

The proton diffusion coefficient.– D_{H^+} (cm^2/s), which appears in Eq. (3), is a measure of the ability of intercalated protons to move within EMD crystals, and more to the point, how fast these protons (and the associated electrons that constitute the discharge current in the oxide phase) are able to vacate the reaction sites at the EMD surface. Fig. 9 shows the effect D_{H^+} has on three individual current spikes in a 5 mV/hr SPECS simulation. We observe, as expected, that changes in D_{H^+}

have little to no effect on the magnitude of the initial current spike. As we have seen, this magnitude is predominantly governed by the i_0^0 value. However, D_{H^+} does greatly influence the ensuing relaxation response. For small D_{H^+} values, for example $1\times10^{-17}\,cm^2/s$, the current almost immediately decreases to below half of its initial value at the potential step. Following this, the current maintains a flatter, more steady response. This corresponds to a diffusion limited process where protons are slow to clear the the surface of the EMD following intercalation. For larger D_{H^+} values, for example $1\times10^{-15}\,cm^2/s$, the current does not experience a large immediate decrease, but rather displays a closer to linear decline. This corresponds to a process where protons are more readily cleared from the EMD surface following intercalation and the current response is limited by the kinetics of the electrochemical reaction at the EMD/KOH interface. In addition, from Fig. 9 we can see that the amount of EMD utilised in a certain time-frame (which is proportional to the area under the current response) is dependent upon the value of D_{H^+}. Such a dependency is exacerbated when diffusion is the limiting process as is the case when D_{H^+} takes the values of 1×10^{-16} and $1\times10^{-17}\,cm^2/s$. We observe that a small D_{H^+} value of $1\times10^{-17}\,cm^2/s$ allows less EMD to be utilised than when D_{H^+} has a value of $1\times10^{-16}\,cm^2/s$. This is expected since D_{H^+} directly influences the availability of reaction sites at the EMD surface.

The SPECS simulation shown in Fig. 9 with a D_{H^+} value of $1\times10^{-16}\,cm^2/s$ seems to match the experimental data for the beginning of each potentiostatic discharge, but none of the simulations match the experimental data at the end of each potentiostatic discharge. The inability of the model to accurately predict the current relaxation curve may be evidence for a concentration dependent D_{H^+} (as has been suggested by Zang, Chen and Xi[31], for example) or multiple D_{H^+} values corresponding to different reduction processes (as is consistent with the multiple reaction picture of Chabre and Pannetier[8]).

Fig. 10 shows the effect of D_{H^+} on the overall discharge behaviour. We previously observed in Fig. 9 that D_{H^+} primarily affects the current relaxation response, and not the minimum and max-

imum current. This is seen to be true in the overall discharge until approximately 1.25 V. Below this voltage, the simulated SPECS discharge with a D_{H^+} value of $1\times10^{-17}\,cm^2/s$ has a larger power response than the other cases shown in the figure. This difference occurs because the cathodes with the larger D_{H^+} values have utilised, or exhausted, most of their EMD, and cannot produce a sizable current response.

Conclusions

A novel model for the potentiostatic discharge of primary alkaline battery cathodes has been presented. The model has been solved using a MATLAB® program that can be run on a desktop computer. A single, mean reaction framework, based on the modified kinetic equation proposed by Chabre and Pannetier[8], has been adopted in this model. We have shown that it is possible to simulate the multi-reaction behaviour of the reduction of EMD, as observed in SPECS experiments, using such a model. To achieve this we used the model to investigate the impact that the form of the ion-ion interaction term, $\Upsilon\left(C_{Mn^{4+}}\right)$, appearing in the modified kinetic equation of Chabre and Pannetier, has on the simulation of cathodic discharge resulting from SPECS experiments and insodoing, developed a suitable functional form for $\Upsilon\left(C_{Mn^{4+}}\right)$. The resulting model has been used to simulate SPECS discharges of button cell cathodes, and the results have been validated and compared with experimental data.

The model has been used to investigate the effects that the initial exchange current density, i_0^0, and the diffusion coefficient for protons in EMD, D_{H^+}, have on SPECS discharge. We found that i_0^0 primarily affects the height of the current spike produced when the potential is stepped, but also influences the relaxation of the cell. Moreover, the model results suggest that the exchange current density should vary within the discharge response associated with individual potential steps in a SPECS test as well as across multiple steps. It was observed that such behaviour is consistent with the idea that individual reduction reactions, within the multi-reaction, reduction behaviour of EMD,

have different initial exchange current densities. In addition, the model results suggest that the value of D_{H^+} does not significantly affect the height of the current spikes observed in a SPECS response. Instead, its primary influence is to change the shape of the current relaxation curve. Furthermore, a small value of D_{H^+} decreases the utilisation of EMD, even at the low discharge rates encountered in SPECS discharges.

Acknowledgements

The authors wish to acknowledge the support of Delta EMD Australia Pty. Limited and in particular, Dr R. P. Williams, during the course of this research.

List of Symbols

a_e	activity of KOH electrolyte solution (mol/cm^3)
C_e	KOH concentration on the macroscopic (cathodic) scale (mol/cm^3)
C_i	concentration of species i per unit volume (mol/cm^3)
$D_{e\infty}$	bulk solution KOH diffusion coefficient (cm^2/s)
D_{H^+}	diffusion coefficient of H^+ in manganese oxide (cm^2/s)
E	equilibrium potential of reaction 1 (V)
E_{cell}	applied cell potential (V)
E^θ	standard potential of reaction 1 (V)
F	Faraday's constant, 96485.309 (C/mol)
i_0^0	exchange current density at $t = 0$ s (A/cm^2)

i_e current per unit cross-sectional area of solution phase (A/cm^2)

i_n transfer current density from oxide phase to electrolyte phase (A/cm^2)

k_2, k_3 constants associated with the determination of σ_{EMD}

r radial coordinate on the microscopic (particle) scale (cm)

r_o effective radius of a manganese oxide particle (cm)

R_{gas} universal gas constant, 8.31451 (J/K.mol)

t time (s)

$t^{\square}_{\mathrm{K}^+}$ transport (transference) number for K^+

T temperature (K)

$\mathbf{v}^{\square}$ volume-average velocity for KOH (cm/s)

$\bar{V}_e$ partial molar volume of electrolyte (cm^3/mol)

$\bar{V}_{\mathrm{H_2O}}$ partial molar volume of $\mathrm{H_2O}$ (cm^3/mol)

$\bar{V}_{\mathrm{Mn^{3+}}}$ partial molar volume of MnOOH (cm^3/mol)

x spatial coordinate on the macroscopic (cathode) scale (cm)

y radial coordinate on the submicroscopic (crystal) scale (cm)

y_o effective radius of a manganese oxide crystal (cm)

Greek

α_a anodic transfer coefficient

α_c cathodic transfer coefficient

ε_{EMD} fraction of total electrode volume that is occupied by porous manganese oxide particles

ε_s fraction of total electrode volume that is void due to spaces between porous manganese oxide and/or graphite particles

$\varepsilon_{s(p)}$ fraction of particle volume that is void due to pores

η local overpotential (V)

κ_e effective solution phase conductivity (S/cm)

λ_m eigenvalues defined by Eq. (5)

σ_{EMD} effective conductivity of the manganese oxide phase (S/cm)

Υ ion-ion interaction term (V)

Subscripts

e electrolyte phase

p microscopic (manganese oxide particle) scale

∞ bulk solution devoid of porous structure

Superscripts

0 state at $t = 0$ s

References

1. N. C. Cahoon and M. P. Korver, *J. Electrochem. Soc.*, **106**, 747 (1959).
2. G. S. Bell and R. Huber, *J. Electrochem. Soc.*, **111**, 1 (1964).
3. A. Kozawa and J. F. Yeager, *J. Electrochem. Soc.*, **112**, 959 (1965).
4. J. McBreen, in *Progress in Batteries & Battery Materials, Vol. 1*, A. Kozawa, A. and R. Brod, Editors, p. 1 (1975).
5. D. A. J. Swinkels, K. E. Anthony P. M. Fredericks and P. R. Osborn, *J. Electroanal. Chem.*, **168**, 433 (1984).
6. H. Zhang, Z. H. Chen and X. Xi, *J. Electrochem. Soc.*, **136**, 2771 (1989).
7. Y. P. Chabre, *J. Electrochem. Soc.*, **138**, 329 (1991).
8. Y. Chabre and J. Pannetier, *Prog. Solid St. Chem.*, **23**, 1 (1995).
9. J-S. Chen and H. Y. Cheh, *J. Electrochem. Soc.*, **140**, 1205 (1993).
10. J-S. Chen and H. Y. Cheh, *J. Electrochem. Soc.*, **140**, 1213 (1993).
11. E. J. Podlaha and H. Y. Cheh, *J. Electrochem. Soc.*, **141**, 15 (1994).
12. E. J. Podlaha and H. Y. Cheh, *J. Electrochem. Soc.*, **141**, 28 (1994).
13. T. W. Farrell, Ph. D. Thesis, Queensland University of Technology, Brisbane, QLD, Australia (1998).
14. Y. Zhang and H. Y. Cheh, *J. Electrochem. Soc.*, **146**, 850 (1999).
15. Y. Zhang and H. Y. Cheh, *J. Electrochem. Soc.*, **146**, 3566 (1999).
16. T. W. Farrell, C. P. Please, D. L. S. McElwain D. A. J. Swinkels, *J. Electrochem. Soc.*, **147**, 4034 (2000).

17. T. W. Farrell and C. P. Please, *J. Electrochem. Soc.*, **152**, A1930 (2005).

18. J. F. Johansen, T. W. Farrell and C. P. Please, *J. Power Sources*, **156**, 645 (2006).

19. J. F. Johansen, Ph. D. Thesis, Queensland University of Technology, Brisbane, QLD, Australia (2007).

20. A. Kozawa and R. A. Powers, *J. Electrochem. Soc.*, **113**, 870 (1966).

21. S. Atlung and T. Jacobsen, *Electrochim. Acta*, **26**, 1447 (1981).

22. W. C. Maskell, J. E. Shaw and F. L. Tye, *J. Power Sources*, **8**, 113 (1982).

23. P. Ruetschi, *J. Electrochem. Soc.*, **135**, 2657 (1988).

24. S. V. Patankar, *Numerical Heat Transfer and Fluid Flow*, Hemisphere (1980).

25. R. L. Burden and J. D. Faires, *Numerical Analysis*, 6th ed., Brooks/Cole (1997).

26. Private Communication with Delta EMD Australia Pty. Limited (2005).

27. G. H. Aylward and T. J. V. Findlay, *SI Chemical Data*, 3rd ed., John Wiley and Sons (1994).

28. S. U. Falk and A. J. Salkind, *Alkaline Storage Batteries*, p. 577, John Wiley and Sons, New York (1969).

29. W. G. Sunu and D. N. Bennion, *J. Electrochem. Soc.*, **127**, 2007 (1980).

30. R. P. Williams, T. N. Andersen, N. J. Bristow, A. R. Gee, G. A. Lawrance, and D. A. J. Swinkels, in *Progress in Batteries & Battery Materials, Vol. 15*, J. C. Nardi, Editor, p. 57 (1995).

31. H. Zhang, Z. H. Chen and X. Xi, *J. Electrochem. Soc.*, **136**, 2771 (1989).

List of Figures

1 Schematic representation of the three size scales described within the model (adapted from Ref. [16]).

2 (Color online) Comparison of a simulated 5 mV/hr SPECS discharge (- - -) using a linear form for $\Upsilon\,(C_{\mathrm{Mn^{4+}}})$, with experimental data (—).

3 A polynomial representation of Υ based on fitting Eq.(4) to experimental, 5 mV/hr, SPECS discharge data.

4 (Color online) A comparison of the minimum and maximum power of a simulated 5 mV/hr SPECS discharge (- - -), obtained using the Υ depicted in Fig. 3, with the corresponding experimental data (—).

5 (Color online) The non-linear form ($\Diamond$) of $\Upsilon\,(C_{\mathrm{Mn^{4+}}})$ obtained from Eq. (23) compared to the linear approximation ($\triangledown$) given by Eq. (21).

6 (Color online) A comparison of the minimum and maximum power of a simulated 5 mV/hr SPECS discharge (- - -) using the form of Υ given in Fig. 5, with experimental data (—).

7 (Color online) A comparison of the current spike shape of simulated 5 mV/hr SPECS discharges with i_0^0 values of 5×10^{-9} (–), 5×10^{-8} (–) and 5×10^{-7} (–) A/cm^2, with experimental data ($\square$).

8 (Color online) A comparison of the minimum and maximum power of simulated 5 mV/hr SPECS discharges with i_0^0 values of 5×10^{-9} ($\cdots$), 5×10^{-8} (- - -) and 5×10^{-7} (—) A/cm^2.

9 (Color online) A comparison of the current spike shape of simulated 5 mV/hr SPECS discharges with $D_{\mathrm{H^+}}$ values of 1×10^{-17} (–), 1×10^{-16} (–) and 1×10^{-15} (–) cm^2/s, with experimental data ($\square$).

10 (Color online) A comparison of the minimum and maximum power of simulated 5 mV/hr SPECS discharges with D_{H^+} values of 1×10^{-17} (···), 1×10^{-16} (- - -) and 1×10^{-15} (—) cm^2/s.

List of Tables

1 Discharge and cell geometry parameters.

2 Physical and kinetic parameters used in the model.

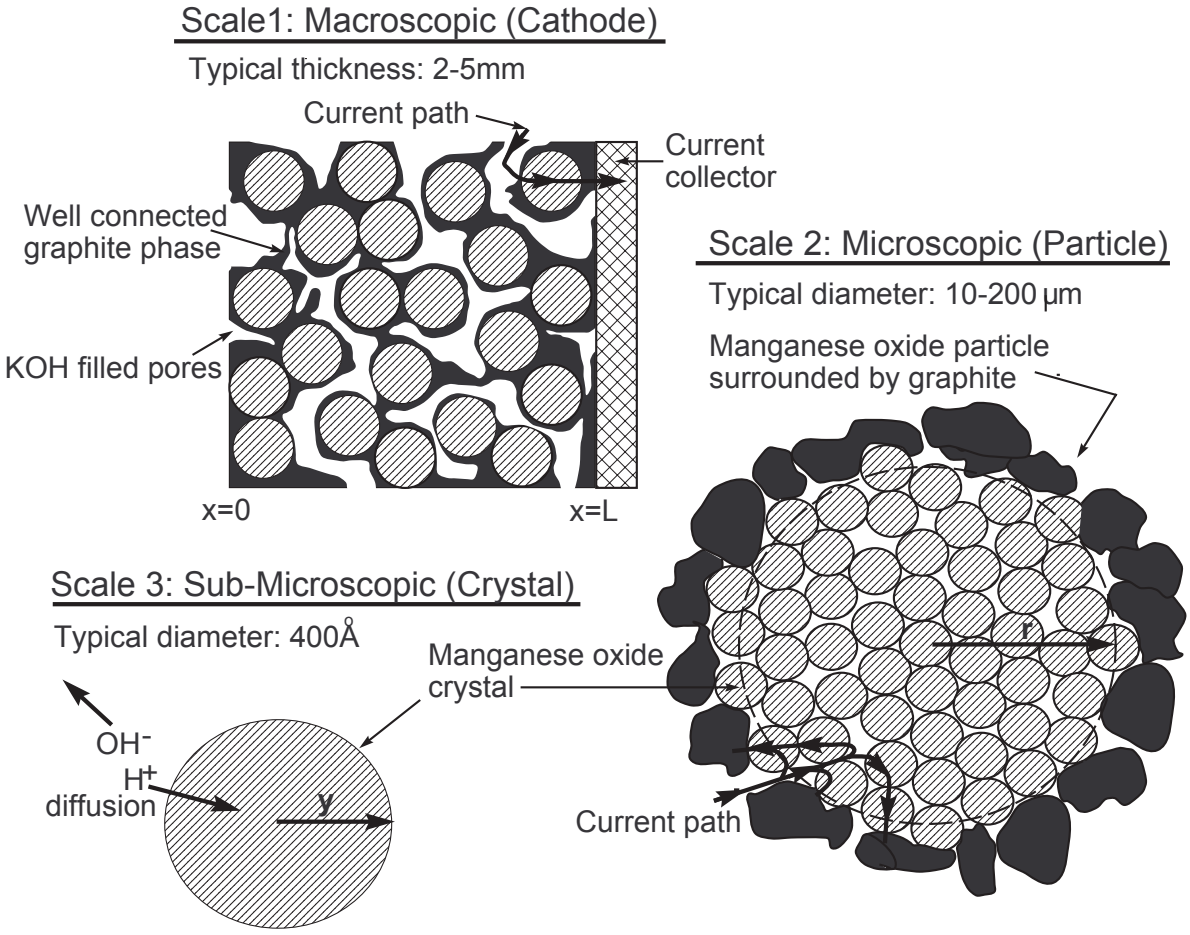
Scale1: Macroscopic (Cathode)
Typical thickness: 2-5mm
Current path
Current collector
Well connected graphite phase
KOH filled pores
x=0
x=L
Scale 2: Microscopic (Particle)
Typical diameter: 10-200 μm
Manganese oxide particle surrounded by graphite
r
Scale 3: Sub-Microscopic (Crystal)
Typical diameter: 400Å
Manganese oxide crystal
OH-
H+
diffusion
y
Current path

Figure 1

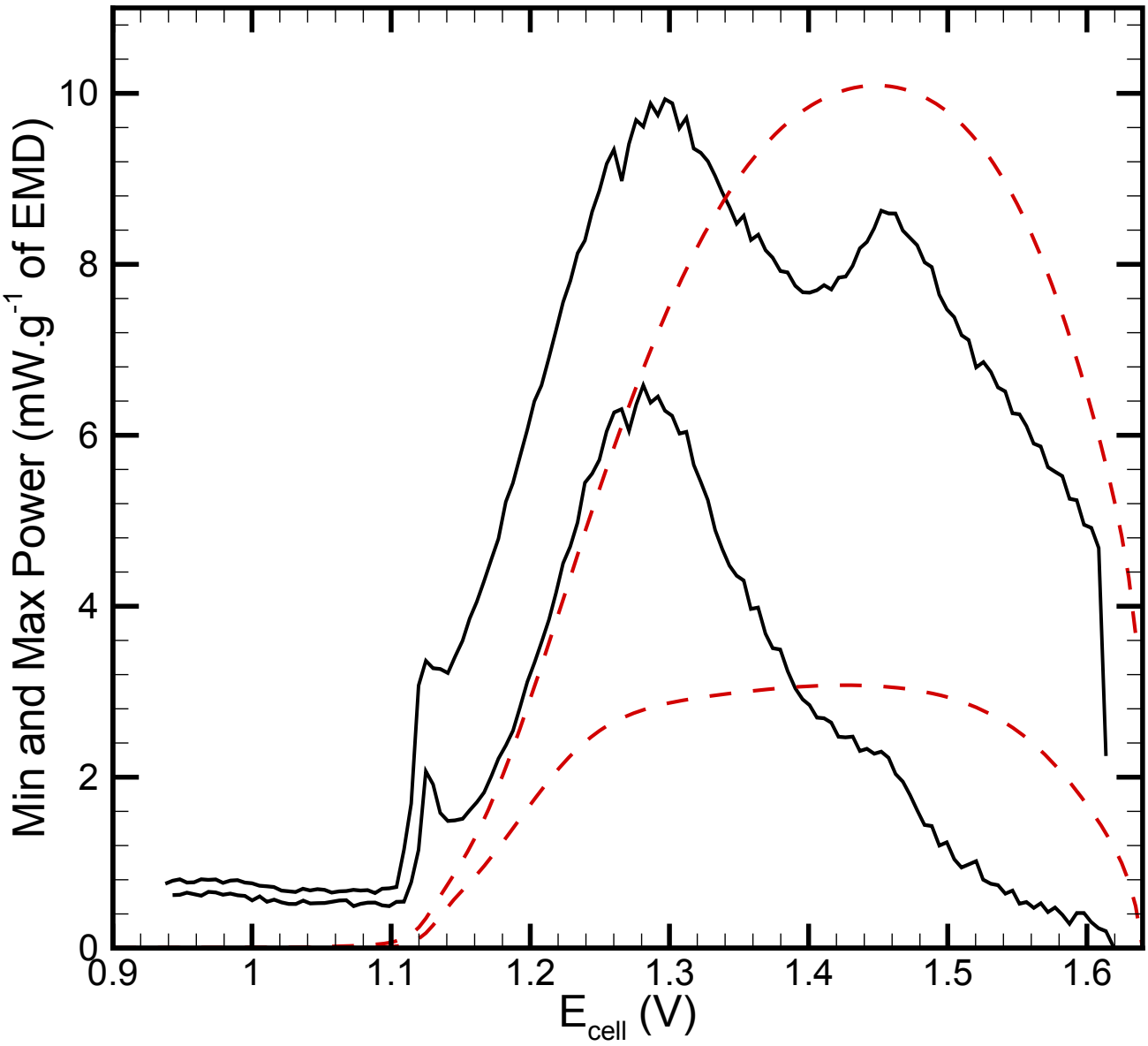
Min and Max Power (mW.g-1 of EMD)
Ecell (V)
0
2
4
6
8
10
0.9
1
1.1
1.2
1.3
1.4
1.5
1.6

Figure 2

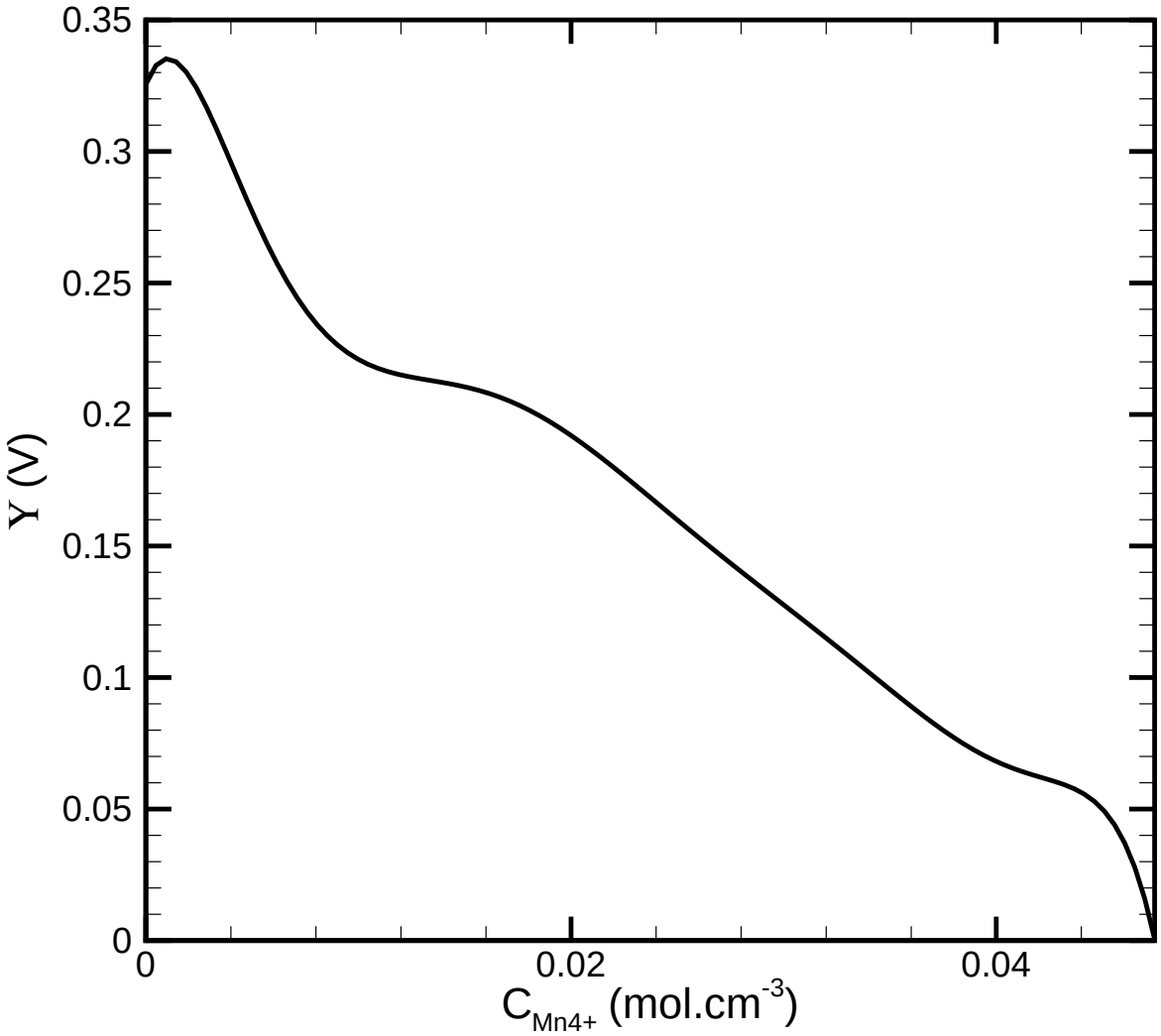

Figure 3

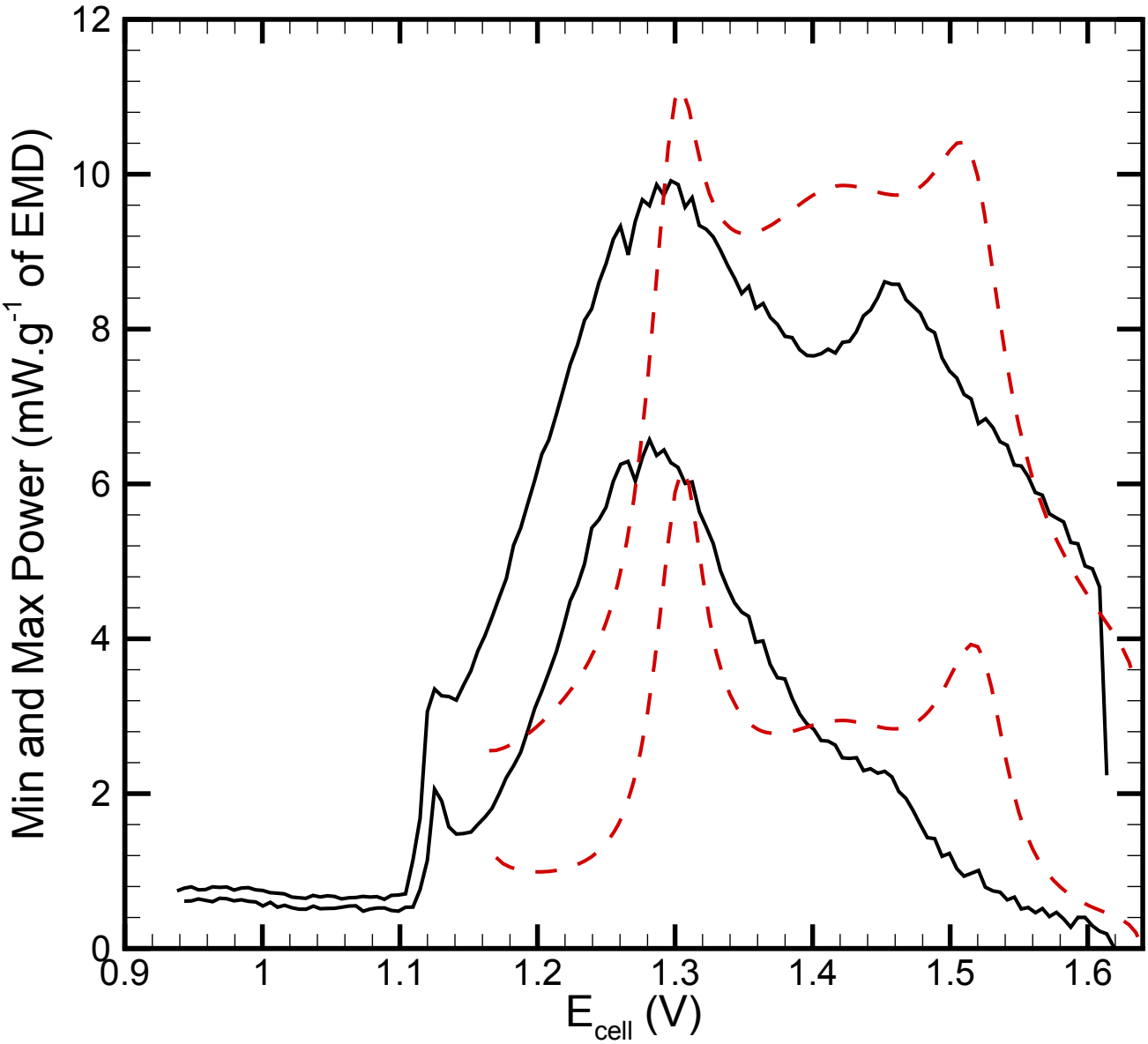
Min and Max Power (mW.g-1 of EMD)
Ecell (V)
0
2
4
6
8
10
12
0.9
1
1.1
1.2
1.3
1.4
1.5
1.6

Figure 4

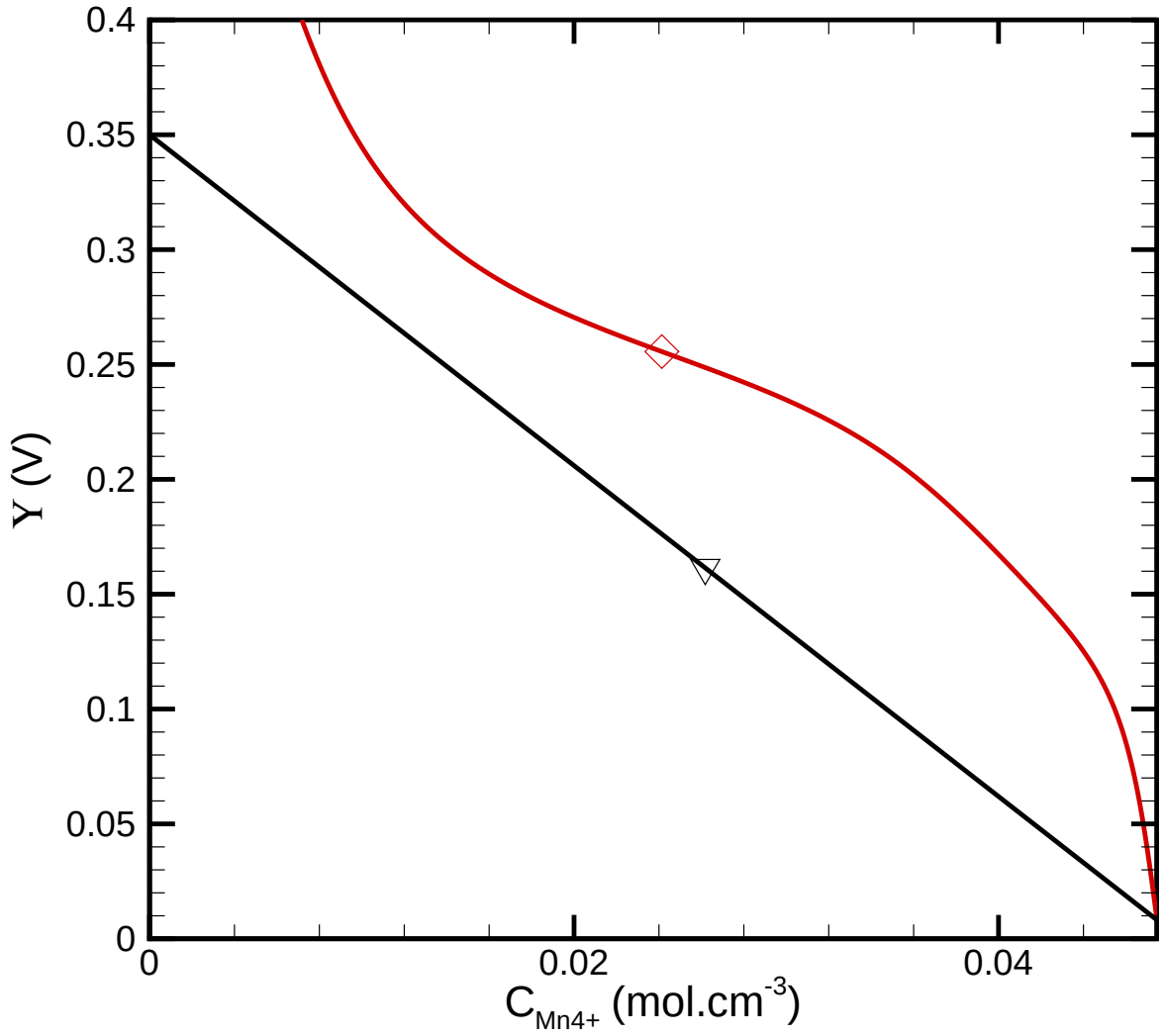

Figure 5

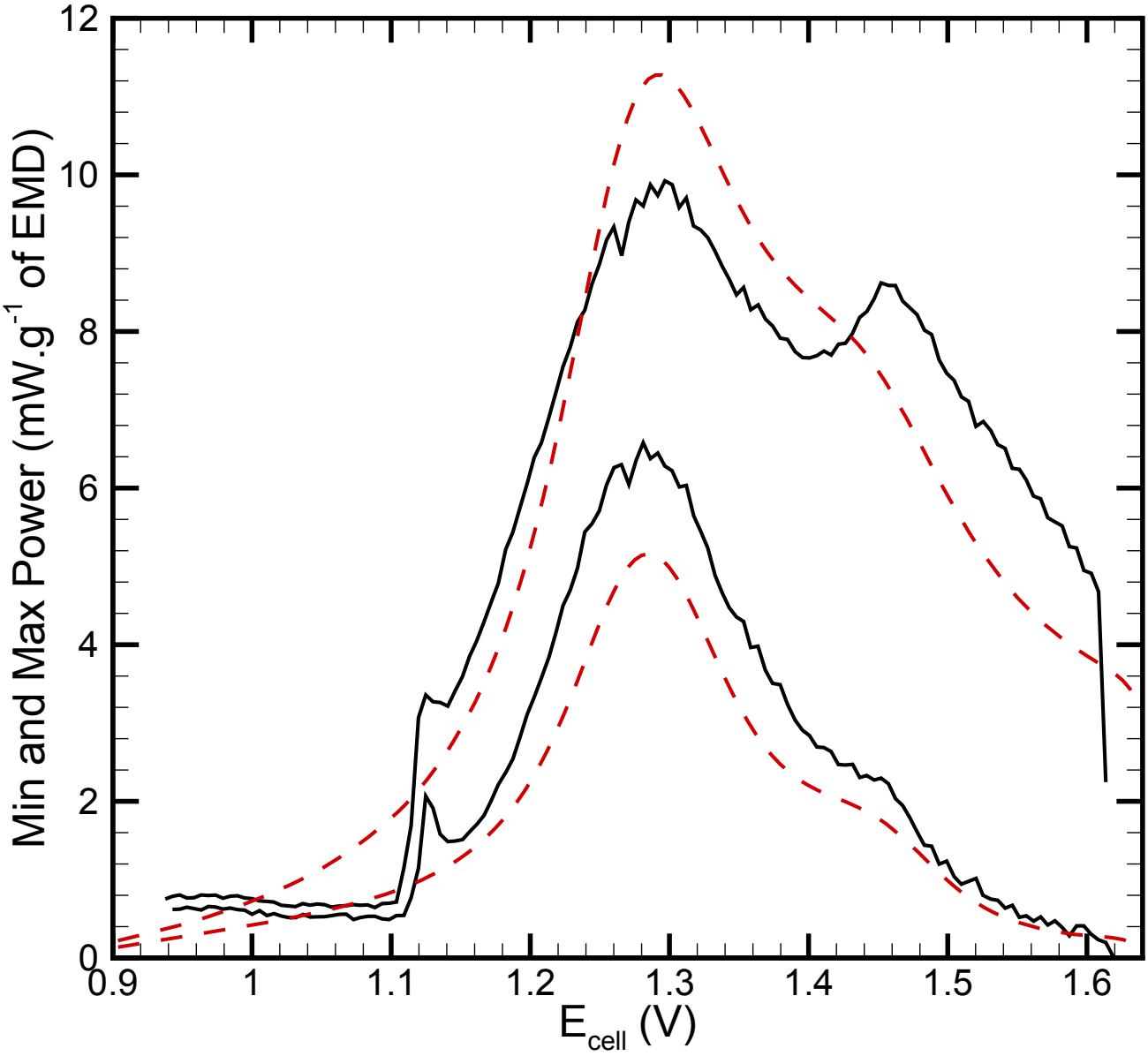
12
10
8
6
4
2
0
0.9
1
1.1
1.2
1.3
1.4
1.5
1.6
Min and Max Power (mW.g-1 of EMD)
Ecell (V)

Figure 6

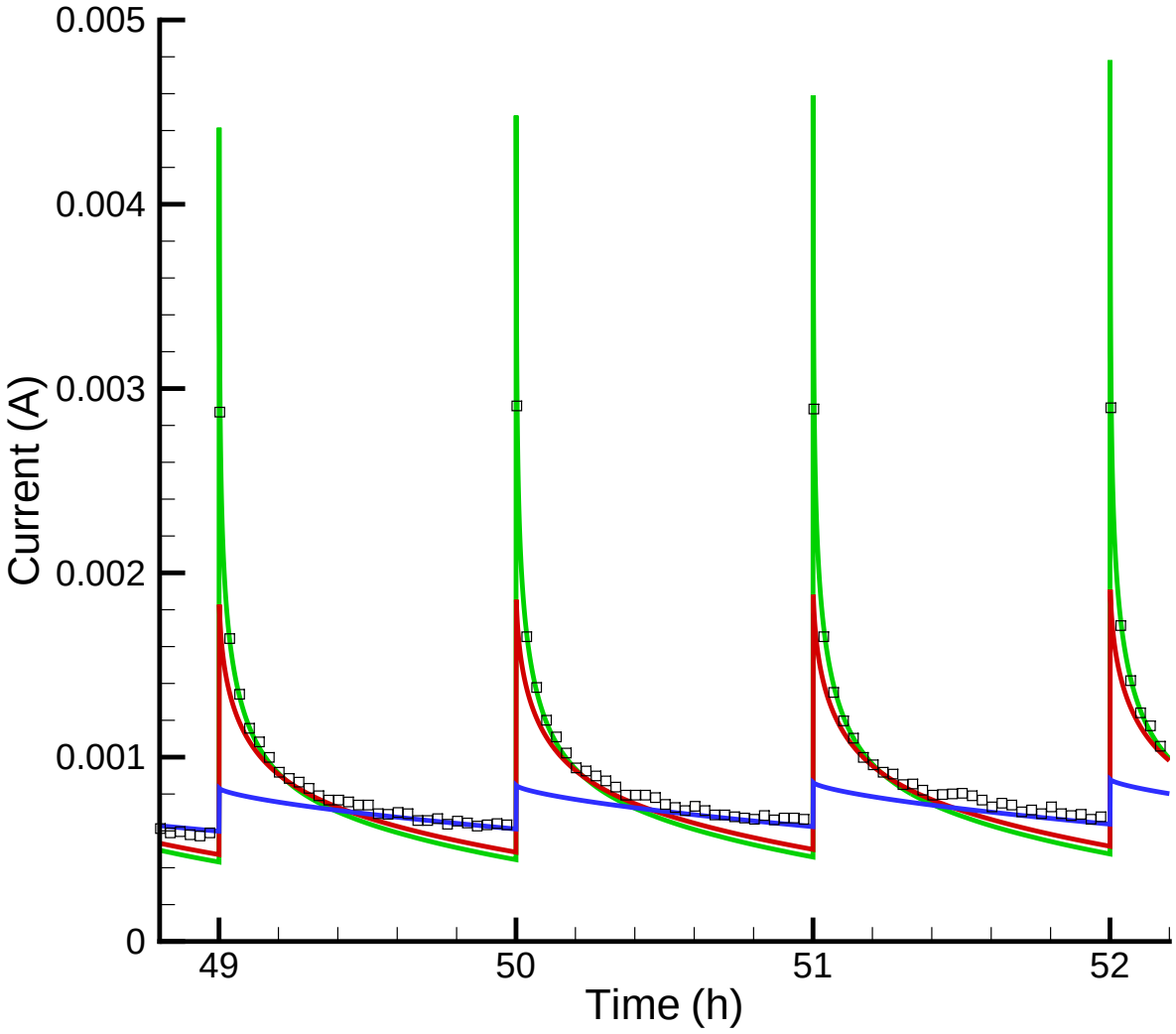

Figure 7

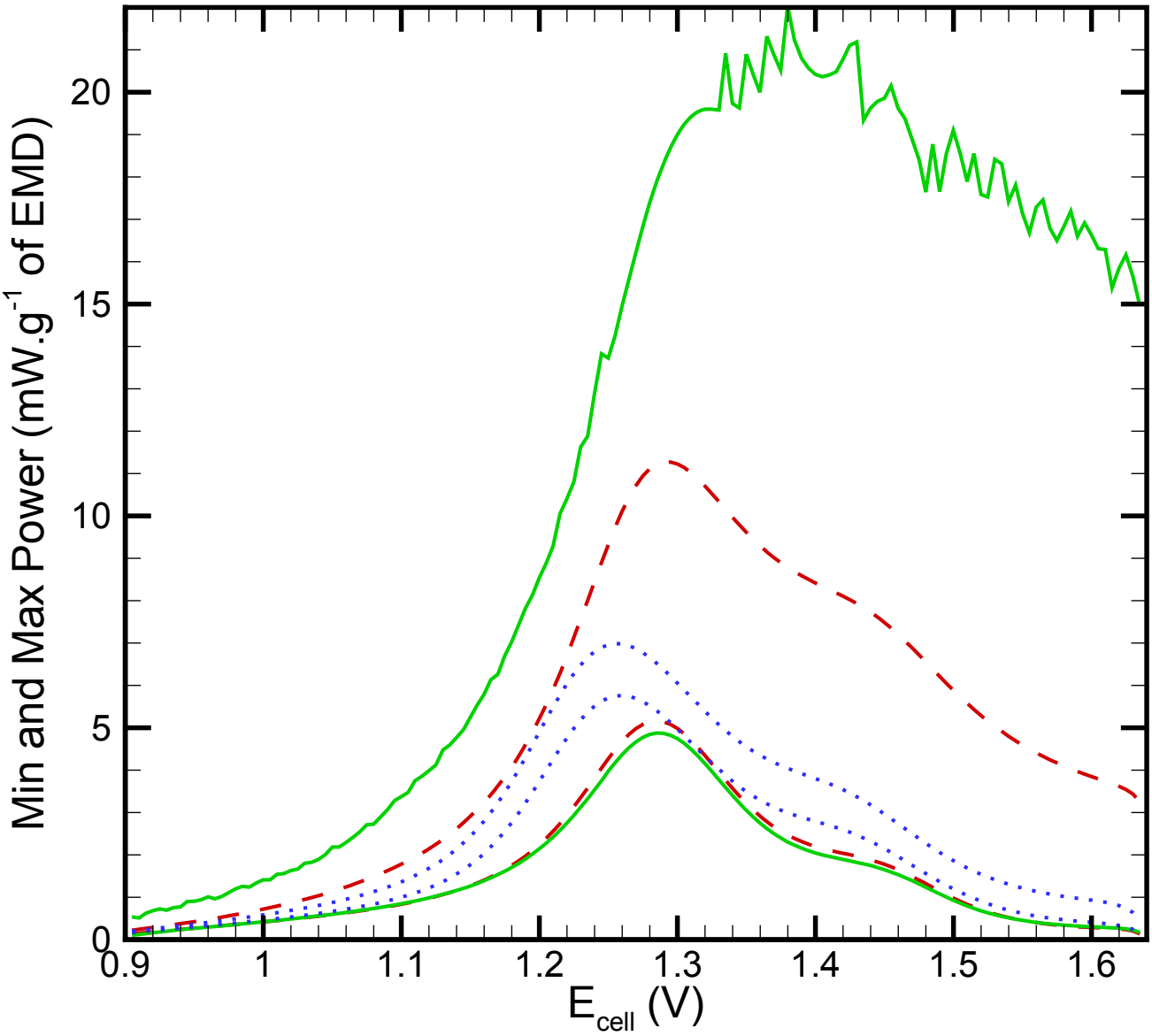
Min and Max Power (mW.g-1 of EMD)
20
15
10
5
0
0.9
1
1.1
1.2
1.3
1.4
1.5
1.6
Ecell (V)

Figure 8

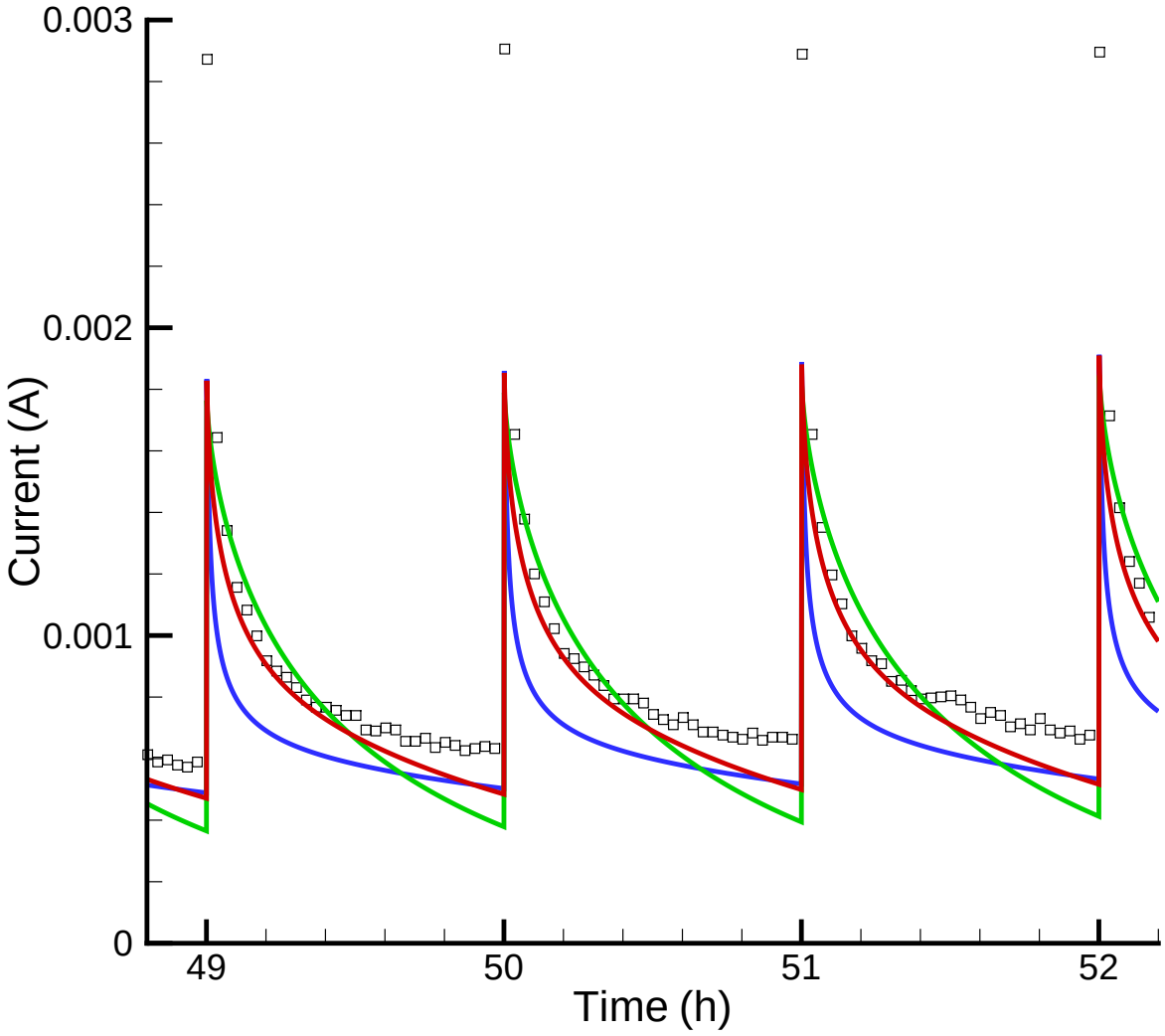

Figure 9

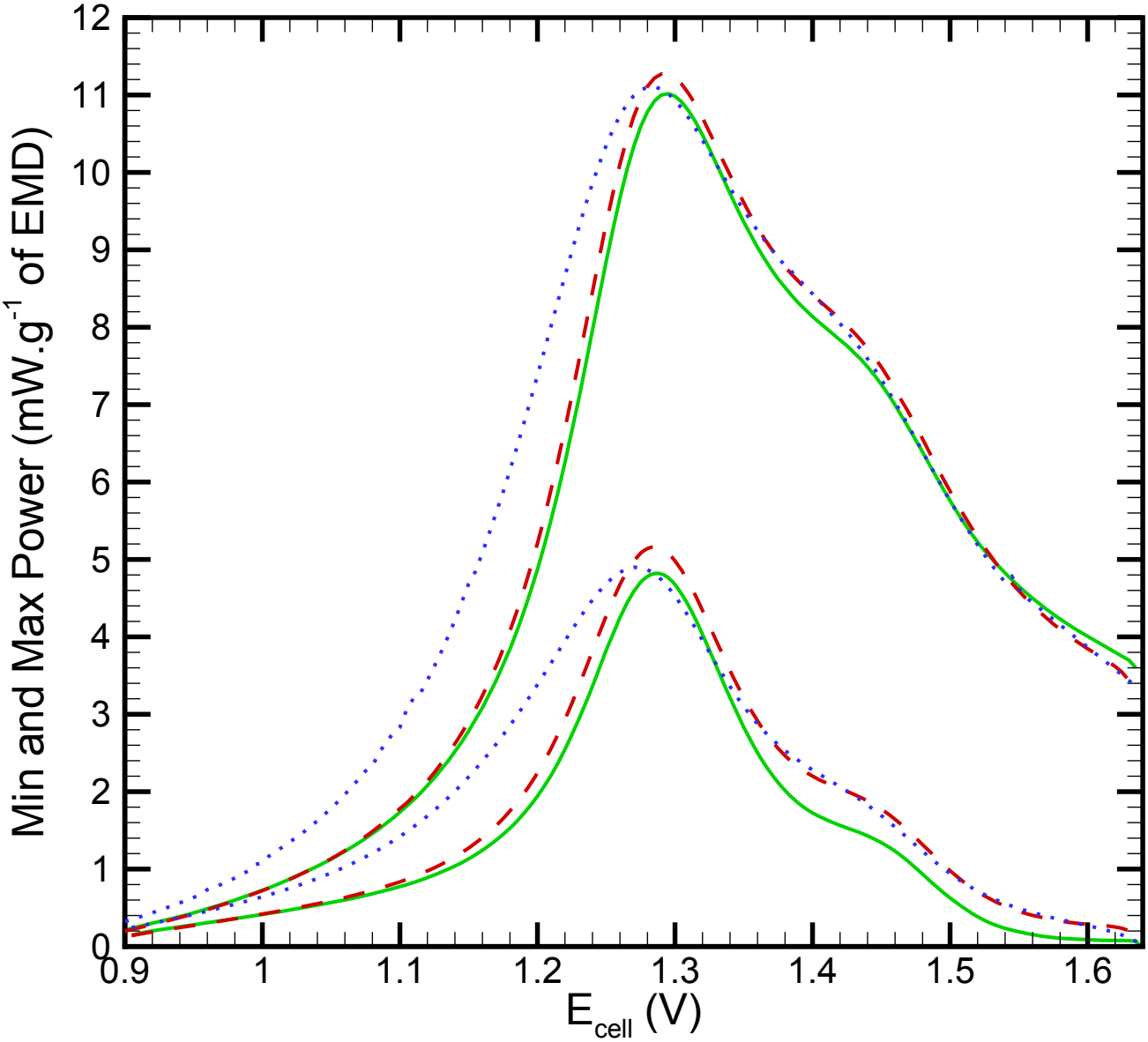
Min and Max Power (mW.g-1 of EMD)
Ecell (V)
0
1
2
3
4
5
6
7
8
9
10
11
12
0.9
1
1.1
1.2
1.3
1.4
1.5
1.6

Figure 10

Table 1

Parameter	Value
Potential step size	5 (mV)
Potential step time	3600 (s)
Cathode thickness, L	0.0928 (cm)
Cathode cross-sectional area	1.732 (cm^2)
Total mass of cathode	0.5 (g)
Mass of EMD in cathode	0.3 (g)
Mass of graphite in cathode	0.175 (g)

Table 2

Parameter	Value and reference
C_e^0	0.009 (mol/cm^3) [26]
$C_{\mathrm{Mn^{4+}}}^0$	0.0486 (mol/cm^3) [16]
$D_{\mathrm{H^+}}$	1×10^{-6} (cm^2/s)
E^0	1.65 (V) [16]
F	96485.309 (C/mol) [27]
i_0^0	5×10^{-8} (A/cm^2) [16]
k_2	1.5×10^2 (S/cm) [18]
k_3	4.328 [18]
R_{gas}	8.31451 (J/K.mol) [27]
r_o	25 (μm) [26]
T	298.15 (K)
$t_{\mathrm{K^+}}^{\square}$	0.22 [28]
$\bar{V}_e$	17.8 (cm^3/mol) [29]
$\bar{V}_{\mathrm{H_2O}}$	18.07 (cm^3/mol) [29]
$\bar{V}_{\mathrm{Mn^{3+}}}$	20.576 (cm^3/mol) [16]
y_o	2.6×10^{-6} (cm) [30]
α_a	0.5
α_c	0.5
$\varepsilon_{\mathrm{EMD}}$	0.61 [16]
ε_s	0.22 [16]
$\varepsilon_{s(p)}$	0.1 [30]